

**Photoabsorption studies of some closed-shell ions in the La isonuclear sequence**Sindhu Kalyadan,<sup>1</sup> Hari R. Varma,<sup>1,\*</sup> P. C. Deshmukh,<sup>1,2</sup> J. T. Costello,<sup>3</sup> P. Hayden,<sup>3</sup> and S. T. Manson<sup>4</sup><sup>1</sup>*School of Basic Sciences, Indian Institute of Technology Mandi, Mandi 175005, India*<sup>2</sup>*Department of Physics and Astronomy, The University of Western Ontario, London, Canada, N6G 3A9*<sup>3</sup>*School of Physical Sciences, Dublin City University, Dublin 9, Ireland*<sup>4</sup>*Department of Physics and Astronomy, Georgia State University, Atlanta, Georgia 30303, USA*

(Received 19 March 2015; published 26 May 2015)

Photoionization cross sections and dipole angular distribution asymmetry parameters,  $\beta$ , of  $5s$  and  $4d$  shells of the closed-shell ions ( $\text{La}^{3+}$ ,  $\text{La}^{9+}$ , and  $\text{La}^{11+}$ ) in the La isonuclear sequence have been studied using the relativistic random phase approximation. The positions of the  $5s$  Cooper minima in  $\text{La}^{3+}$  and  $\text{La}^{9+}$  ions are found to be extremely sensitive to the details of electron correlation. The results show that the  $5s$  cross sections of  $\text{La}^{3+}$  and  $\text{La}^{9+}$  do not lie along the same curve near the thresholds; the  $4d$  cross sections, however, do match well in overlap regions so they lie along the same curve, over the isonuclear sequence, except for a shift in threshold towards higher energies with increasing degree of ionization.

DOI: [10.1103/PhysRevA.91.053422](https://doi.org/10.1103/PhysRevA.91.053422)

PACS number(s): 32.80.Fb

**I. INTRODUCTION**

A fundamental understanding of laser plasma emission and absorption mechanisms in the vicinity of 6.5–6.9 nm is important as spectral transitions in this region offer themselves as good candidates for next generation Extreme Ultraviolet (EUV) lithography (EUVL) [so-called 6.x nm lithography, or beyond-EUV lithography (BEUVL)], due to the availability of high-reflectivity ( $\sim 60\%$ ) La/B<sub>4</sub>C multilayer mirrors at these wavelengths [1]. Studies in this wavelength range could help determine the conditions for optimum conversion efficiency from a high-power laser driver to 6.x nm wavelength plasma emission. This would be a key benchmark in determining the economic viability for deployment of any EUVL source solution in high-volume manufacturing. Novel target configurations need to be explored towards gaining control in engineering plasma conditions to optimize the conversion efficiency, with transitions in Ag-, Pd-, and Rh-like ion stages of Gd and Tb the most promising to date [2,3]. We explore some ions among the lanthanides in an energy range overlapping with the energy region of interest for EUVL. We have chosen a few ions from the La isonuclear sequence to study their photoionization using the relativistic random phase approximation (RRPA), as La provides the material most suitable for producing high-reflectivity multilayer mirrors for the next generation of EUVL, and also La provides access to isoelectronic ion stages of the potential sources.

In addition, from a basic physics point of view, photoionization of multiply charged ions is of great interest in studying electron correlations and relativistic effects. Both resonant and nonresonant processes resulting from atomic or ionic photoabsorption are of interest [4]. Photoionization data are also very valuable in atmospheric physics, astrophysics, inertial confinement, and tokamak fusion energy studies [5–9]. A number of photoionization measurements of outer shells of isonuclear sequences for Xe, Cs, Ba, Fe, and Ce have been reported [10–14]. Theoretical calculations based on the Hartree-Slater and Dirac-Slater methods have been reported for the O, Fe, Hg isonuclear sequences [15–17]. Photoionization of the

inner shells of the Mg, Ar, and Ca isonuclear sequences [18–20] using the relativistic random phase approximation (RRPA) [21] has also been reported earlier. These studies showed that removal of electrons from a subshell having a higher principal quantum number does not have any effect on the inner-shell photoionization cross sections, except for a shift in the photoionization threshold to higher energies. However, along an isonuclear sequence, the angular distribution asymmetry parameter of the photoelectrons was found to show a different behavior near the thresholds due to its dependency on the Coulomb phase shift [20] which scales differently.

In the present work, we have chosen three multiply charged ions of the La ( $Z = 57$ ) isonuclear sequence.  $\text{La}^{3+}$ ,  $\text{La}^{9+}$ , and  $\text{La}^{11+}$  were chosen since they have closed-shell electron configurations and can therefore be studied using the RRPA [21]; the ground-state structures of these ions are  $[\text{Kr}]4d^{10}5s^25p^6$ ,  $[\text{Kr}]4d^{10}5s^2$ , and  $[\text{Kr}]4d^{10}$ , respectively. Photoionization of these ions is studied in the energy range 2.5–15 a.u. (ca. 70–400 eV or 18–3 nm, respectively), which includes the region of current interest in the technology of next generation EUVL. EUV emission spectra of higher members of the La isonuclear sequence ( $\text{La}^{11+}$  to  $\text{La}^{20+}$ ) have been reported in work by Kilbane and O’Sullivan [22]. They studied the transitions in the wavelength range 8.5–10.5 nm (5.4–4.4 a.u.) [22]. In this paper we report a study of photoionization cross sections as well as angular distribution parameters for  $5s$  and  $4d$  photoelectrons. These studies provide information about the energy range where bound-bound transitions can occur. In the present work, our focus is first on the study of the background (nonresonant) photoionization parameters; the autoionizing resonances will be studied separately using the relativistic multichannel quantum defect theory (RMQDT) [23]. Photoionization of inner  $4d$  shells for Xe-like ions (Xe, Cs<sup>+</sup>, Ba<sup>2+</sup>, and La<sup>3+</sup>) using RRPA has been reported earlier [24]. The photoabsorption spectrum of La<sup>3+</sup> ion in the  $4d$  excitation region using the dual laser-produced plasma (DLP) technique has also been reported [25,26].

**II. THEORY**

The relativistic random phase approximation (RRPA) [21] is a many-body theory, which includes electron correlations

\*Corresponding author: hari@iitmandi.ac.in

and relativistic effects. Electron correlations in the initial state of the atomic photoionization process are built into the technique through time-backward ring diagrams (and corresponding exchange diagrams) over the Dirac-Hartree-Fock (DHF) wave functions and are essentially mixing of the initial state with two-particle two-hole excitation configurations. Correlations in the final state of the photoionization process are included through time-forward ring diagrams and amount to including interchannel coupling in the photoionization. The DHF threshold values used in our RRPA calculation are presented in Table I. In the present work, dipole channels arising from deep inner shells are omitted, and thus we have applied a truncation of the RRPA method, which results in small differences between the length and velocity forms of the transition matrix elements.

In the RRPA, the photoionization cross section for subshell  $(n, \kappa)$  is given by [21]

$$\sigma_{n,\kappa}(\omega) = \frac{4\pi^2\alpha\omega}{3} (|D_{nj \rightarrow j-1}|^2 + |D_{nj \rightarrow j}|^2 + |D_{nj \rightarrow j+1}|^2), \quad (1)$$

where  $D_{nj \rightarrow j'}$  represents the reduced dipole matrix element between an initial-state orbital  $(n, \kappa_b)$  and a continuum orbital  $(\varepsilon, \kappa_c)$ , and is given by [27]  $D_{nj \rightarrow j'} = i^{l-l'} e^{i\delta_\kappa} \langle \kappa || Q_1^{(l)} || \kappa_b \rangle$ . Here  $\delta_\kappa$  and  $l$  represent the phase shift and the orbital angular momentum quantum number of the continuum state, respectively, while  $\omega$  is the photon energy.

TABLE I. Calculated Dirac-Hartree-Fock (DHF) subshell binding energies in a.u.

Subshell	La <sup>3+</sup>	La <sup>9+</sup>	La <sup>11+</sup>
1s <sub>1/2</sub>	1439.85	1443.652	1445.24
2s <sub>1/2</sub>	233.835	237.585	239.13
2p <sub>1/2</sub>	219.97	223.73	225.29
2p <sub>3/2</sub>	204.74	208.49	210.05
3s	52.37	56.06	57.577
3p <sub>1/2</sub>	46.50	50.186	51.713
3p <sub>3/2</sub>	43.46	47.142	48.668
4s	11.97	15.55	16.985
3d <sub>3/2</sub>	33.30	37.003	38.537
3d <sub>5/2</sub>	32.66	36.36	37.894
4p <sub>1/2</sub>	9.722	13.28	14.739
4p <sub>3/2</sub>	9.070	12.62	14.076
4d <sub>3/2</sub>	5.305	8.855	10.298
4d <sub>5/2</sub>	5.190	8.738	10.180
5s	2.635	5.515	
5p <sub>1/2</sub>	1.926		
5p <sub>3/2</sub>	1.822		

The dipole angular distribution asymmetry parameter  $\beta$  of the photoelectrons results from the interference between various electric dipole amplitudes [21] and is given by

$$\begin{aligned} \beta_{n\kappa}(\omega) = & \left\{ \frac{(2j-3)}{2(2j)} |D_{j \rightarrow j-1}|^2 - \frac{(2j-1)(2j+3)}{(2j)(2j+2)} |D_{j \rightarrow j}|^2 + \frac{(2j+5)}{2(2j+2)} |D_{j \rightarrow j+1}|^2 \right. \\ & - \frac{3}{2j} \left[ \frac{(2j-1)}{2(2j+2)} \right]^{\frac{1}{2}} [D_{j \rightarrow j-1} D_{j \rightarrow j}^* + \text{c.c.}] - \frac{3}{2} \left[ \frac{(2j-1)(2j+3)}{2j(2j+2)} \right]^{\frac{1}{2}} [D_{j \rightarrow j-1} D_{j \rightarrow j+1}^* + \text{c.c.}] \\ & \left. + \frac{3}{(2j+2)} \left[ \frac{(2j+3)}{2(2j)} \right]^{\frac{1}{2}} [D_{j \rightarrow j} D_{j \rightarrow j+1}^* + \text{c.c.}] \right\} \\ & \times \{ |D_{j \rightarrow j-1}|^2 + |D_{j \rightarrow j}|^2 + |D_{j \rightarrow j+1}|^2 \}^{-1}, \quad (2) \end{aligned}$$

where ‘‘c.c.’’ represents the complex conjugate.

To study the effects of interchannel coupling on the 5s photoionization in La<sup>3+</sup> and La<sup>9+</sup> in detail, several different levels of truncation of the RRPA calculations were performed to allow us to pinpoint the effect(s) of each of the couplings. Specifically, the following truncations were utilized for each ion stage:

La<sup>3+</sup> case:

- 2 channels: 5s<sub>1/2</sub> → p<sub>3/2</sub>, p<sub>1/2</sub>
- 5 channels: 5s<sub>1/2</sub> → p<sub>3/2</sub>, p<sub>1/2</sub>, 4d<sub>3/2</sub> → p<sub>3/2</sub>, p<sub>1/2</sub>, f<sub>5/2</sub>
- 5 channels: 5s<sub>1/2</sub> → p<sub>3/2</sub>, p<sub>1/2</sub>, 4d<sub>5/2</sub> → p<sub>3/2</sub>, f<sub>5/2</sub>, f<sub>7/2</sub>
- 8 channels: 5s<sub>1/2</sub> → p<sub>3/2</sub>, p<sub>1/2</sub>, 4d<sub>5/2</sub> → p<sub>3/2</sub>, f<sub>5/2</sub>, f<sub>7/2</sub>, 4d<sub>3/2</sub> → p<sub>3/2</sub>, p<sub>1/2</sub>, f<sub>5/2</sub>
- 13 channels: 5p<sub>3/2</sub> → d<sub>5/2</sub>, d<sub>3/2</sub>, s<sub>1/2</sub>, 5p<sub>1/2</sub> → d<sub>3/2</sub>, s<sub>1/2</sub>, 5s<sub>1/2</sub> → p<sub>3/2</sub>, p<sub>1/2</sub>, 4d<sub>5/2</sub> → p<sub>3/2</sub>, f<sub>5/2</sub>, f<sub>7/2</sub>, 4d<sub>3/2</sub> → p<sub>3/2</sub>, p<sub>1/2</sub>, f<sub>5/2</sub>

La<sup>9+</sup> case:

- 2 channels: 5s<sub>1/2</sub> → p<sub>3/2</sub>, p<sub>1/2</sub>
- 5 channels; 5s<sub>1/2</sub> → p<sub>3/2</sub>, p<sub>1/2</sub>, 4d<sub>3/2</sub> → p<sub>3/2</sub>, p<sub>1/2</sub>, f<sub>5/2</sub>
- 5 channels: 5s<sub>1/2</sub> → p<sub>3/2</sub>, p<sub>1/2</sub>, 4d<sub>5/2</sub> → p<sub>3/2</sub>, f<sub>5/2</sub>, f<sub>7/2</sub>
- 8 channels: 5s<sub>1/2</sub> → p<sub>3/2</sub>, p<sub>1/2</sub>, 4d<sub>5/2</sub> → p<sub>3/2</sub>, f<sub>5/2</sub>, f<sub>7/2</sub>, 4d<sub>3/2</sub> → p<sub>3/2</sub>, p<sub>1/2</sub>, f<sub>5/2</sub>

La<sup>11+</sup> case:

6 channels: 4d<sub>5/2</sub> → p<sub>3/2</sub>, f<sub>5/2</sub>, f<sub>7/2</sub>, 4d<sub>3/2</sub> → p<sub>3/2</sub>, p<sub>1/2</sub>, f<sub>5/2</sub>.

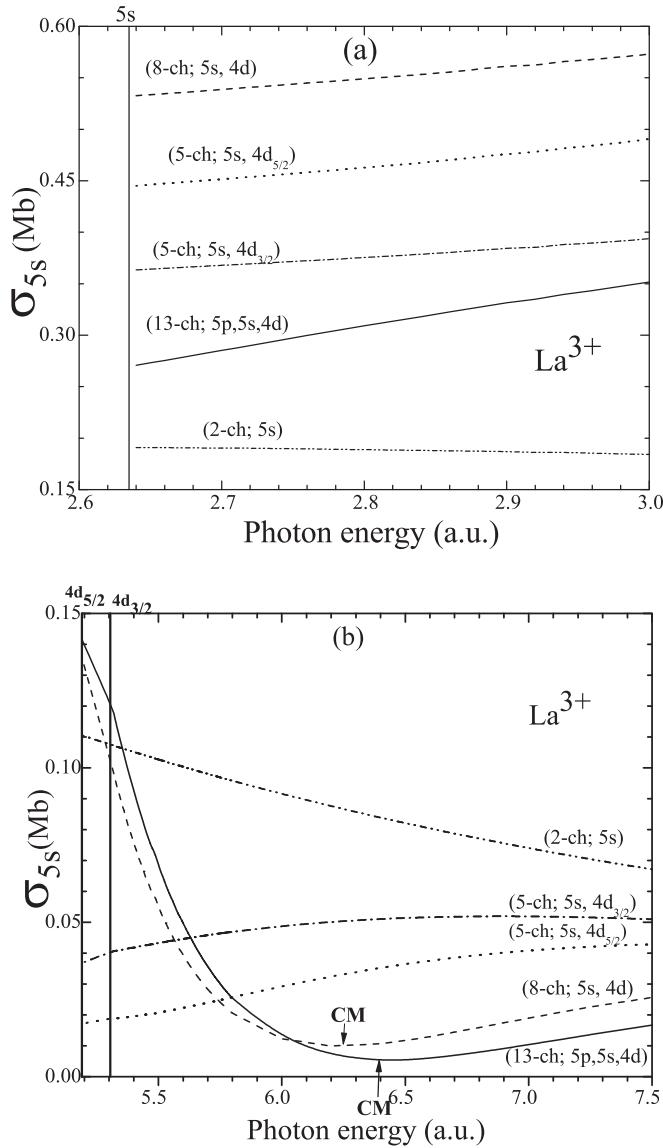


FIG. 1.  $5s$  photoionization cross sections,  $\sigma_{5s}$ , for  $\text{La}^{3+}$  calculated at various levels of truncation of the RRPAs with each cross section labeled by the number of channels and the subshells included, and thresholds labeled and indicated by vertical lines for energies (a) 2.6–3.0 a.u., (b) 5.2–7.5 a.u. CM refers to the location of the Cooper minimum.

### III. RESULTS AND DISCUSSION

The  $5s$  photoionization cross sections for the  $\text{La}^{3+}$  ion, calculated using the RRPAs with different levels of truncation, are shown in Figs. 1(a) and 1(b) for the threshold and intermediate energy regions, respectively; the region between 3 and 5.2 a.u. is omitted as it is dominated by resonances. The 2-channel result does not include interchannel coupling with the photoionization cross sections from other subshells, and it shows a monotonic decrease from threshold. Since this result, although including interchannel coupling between  $s \rightarrow p_{1/2}$  and  $s \rightarrow p_{3/2}$  spin-orbit split continua, does not address correlations resulting from photoionization of the atom from other subshells, it is akin, to a significant extent, to what one may expect from a single-particle approximation. However,

when interchannel coupling with photoionization channels from other subshells are included, the result is significantly altered in the sense that the cross section does not exhibit the simple monotonic behavior as in the 2-channel result, as well as differences in the magnitude.

As seen in Fig. 1(a), the two 5-channel ( $5s + 4d_{3/2}$  and  $5s + 4d_{5/2}$ ) results, the 8-channel ( $5s + 4d$ ), and the 13-channel ( $5p + 5s + 4d$ ) results show an increase, if only a gentle one, of the cross section above threshold indicating that, with the coupling, the  $5s$  Cooper minimum lies in the discrete region below the  $5s$  threshold. In addition, Fig. 1(b) shows that both of the 5-channel coupled  $5s$  cross sections, in which the truncated RRPAs have employed interchannel coupling between the two relativistic dipole channels from the  $5s$  with three relativistic dipole channels from either  $4d_{5/2}$  or  $4d_{3/2}$ , show an increase of the  $5s$  cross section above the  $4d$  thresholds, indicating the presence of an additional Cooper minimum below the  $4d$  thresholds due to the coupling. The exact position of this second Cooper minimum is not shown in the figure, because background-photoionization parameters in this region are strongly modulated by the presence of autoionizing resonances resulting from the interference with  $4d \rightarrow np, nf$  (bound-bound) resonances.

Figure 1(b) also shows the results of the 8-channel coupled truncated RRPAs calculation in which dipole channels from the  $5s$ ,  $4d_{3/2}$ , and  $4d_{5/2}$  subshells are included. The 8-channel result has an additional correlation beyond that addressed in the two separate 5-channel calculations, ( $5s + 4d_{3/2}$  and  $5s + 4d_{5/2}$ ). The Cooper minimum hinted at in the two separate 5-channel calculations now moves to higher energy, above the  $4d$  thresholds, and is seen at  $\sim 6.25$  a.u., indicated by the arrow in Fig. 1(b). The interchannel coupling between channels from the spin-orbit split  $4d$  levels thus has an interesting effect on the  $5s$  cross section; it is responsible for moving the two separate 5-channel coupled results for the  $5s$  Cooper minimum to a higher energy, above the  $4d$  subshells. It is interesting to note from this result that not only is the correlation resulting from coupling of the  $4d$  channels with those from the  $5s$  important, but the interchannel coupling between the relativistic dipole channels from the spin-orbit split  $4d$  subshell is also important in locating the  $5s$  Cooper minimum above the  $4d$  thresholds. The net effect is then somewhat similar to the “spin-orbit-interaction activated interchannel coupling” (SOIAC) effect [28], since the interchannel coupling between channels from the spin-orbit split subshells is crucial.

Inclusion of additional interchannel coupling with channels from the  $5p$  subshells moves the position of this ‘induced’ Cooper minimum to a still higher energy ( $\sim 6.4$  a.u.), as seen in the result for the 13-channel truncated RRPAs curve shown in Fig. 1(b). The actual position of the  $5s$  Cooper minimum is, thus, found to be extremely sensitive to the correlations resulting from interchannel coupling with all of the photoionization channels arising from subshells with nearby thresholds; interchannel coupling with channels arising from deep inner shells have negligible effect, however.

In the dipole photoionization studies of several atoms (Mg, Ca, Ba, Sr, Hg) it was found that interchannel coupling shifts the position of the Cooper minimum to a lower photon energy [29,30]. However, in a recent study of  $3s$  photoionization of the Cl<sup>-</sup> ion [31], it was found that increasing the interchannel

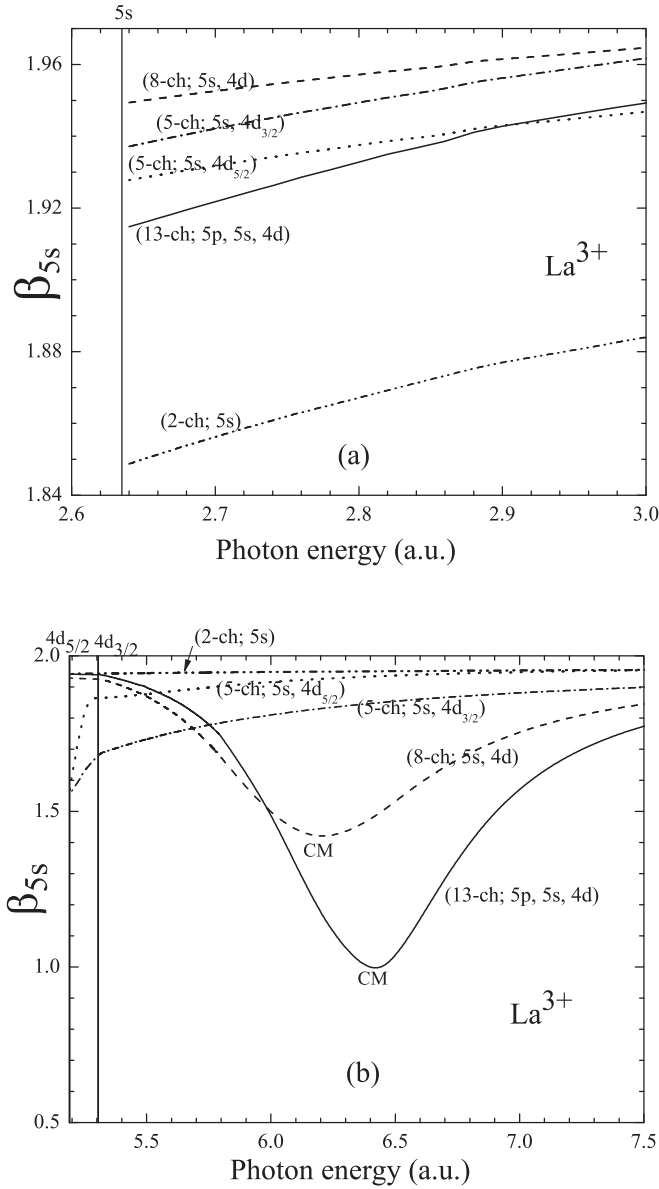


FIG. 2. Same as Fig. 1 but for the photoelectron angular distribution asymmetry parameter,  $\beta_{5s}$ .

coupling shifted the position of the Cooper minimum to higher energy. The present case is similar.

It is well known that in the vicinity of a Cooper minimum, the dipole angular distribution asymmetry parameter,  $\beta$ , for a  $ns$  subshell deviates from its nonrelativistic value of 2 [32,33].  $\beta_{5s}$  for  $\text{La}^{3+}$ , determined for the different levels of truncation in the RRPAs, are shown in Figs. 2(a) and 2(b). As seen from Fig. 2(a), at all levels of truncation, including the 2-channel calculations,  $\beta_{5s}$  deviates from the nonrelativistic value of 2 near the  $5s$  threshold. The 2-channel result for  $\beta_{5s}$  approaches 2 with increasing photon energies, as seen in Fig. 2(b). This observation confirms that the 2-channel result does not suggest the presence of any additional Cooper minima above the threshold, in agreement with the conclusion drawn from the monotonic decrease in the 2-channel cross section,  $\sigma_{5s}$ . The deviation near the threshold is due to the presence of the Cooper minimum in the discrete region.

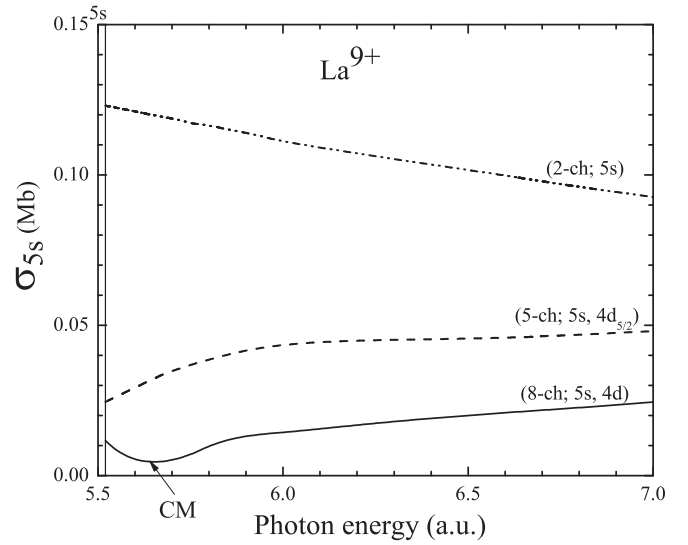


FIG. 3. Same as Fig. 1 but for  $\text{La}^{9+}$  in the 5.5–7.0 a.u. energy range.

As the photon energy increases above the threshold, the two 5-channel coupled calculations ( $5s + 4d_{3/2}$ ,  $5s + 4d_{5/2}$ ) also show that  $\beta_{5s}$  approaches the value of 2, albeit more slowly than the 2-channel result. However,  $\beta_{5s}$  exhibits a different behavior when further interchannel coupling is introduced. Of great interest is the result for  $\beta_{5s}$  obtained by the interchannel coupling from 8 channels; those from the  $5s$ ,  $4d_{3/2}$ , and  $4d_{5/2}$  subshells. Figure 2(b) shows a clear dip in  $\beta_{5s}$  at about 6.25 a.u., suggesting the occurrence of a second Cooper minimum, induced by interchannel coupling—not just between channels from  $5s$  and  $4d_{5/2}$  or  $4d_{3/2}$ , but by the spin-orbit-interaction activated interchannel coupling or SOIAIC effect caused by interchannel coupling between relativistic dipole channels from  $5s$ ,  $4d_{5/2}$ , and  $4d_{3/2}$  [34]. As in the case of the  $5s$  photoionization cross section,  $\beta_{5s}$  also shows that the interchannel coupling induced Cooper minimum moves to an even higher energy ( $\sim 6.4$  a.u.) when additional dipole channels (from the  $5p$  subshell) are coupled. Thus, it is clear that interchannel coupling with all of the relativistic  $5p$  and  $4d$  photoionization channels is required to obtain quantitatively correct results for both the cross section and the asymmetry parameter.

Next we investigate  $\text{La}^{9+}$  which has a  $5s^2$  closed-shell ground-state electron configuration, i.e., as compared to the  $\text{La}^{3+}$  ion, the six  $5p$  electrons are absent. The  $5s$  photoionization cross sections for the  $\text{La}^{9+}$  ion, determined by different levels of truncation, are shown in Fig. 3. As in the case of  $\text{La}^{3+}$ , the 2-channel calculations here also display a monotonic decrease with increasing energy above the  $5s$  threshold. However, the 5-channel ( $5s + 4d_{5/2}$ ) calculation shows an increase in the cross section above the threshold; the other 5-channel ( $5s + 4d_{3/2}$ ) calculation (not shown) behaves similarly. This again indicates the presence of a Cooper minimum in the discrete region. The 8-channel  $\sigma_{5s}$  exhibits a Cooper minimum at  $\sim 5.6$  a.u., induced by spin-orbit activated interchannel coupling. The angular distribution asymmetry parameter for  $\text{La}^{9+}$   $5s$  photoionization is shown in Fig. 4. The results for  $\beta_{5s}$  corroborate the conclusion, stated above, that interchannel

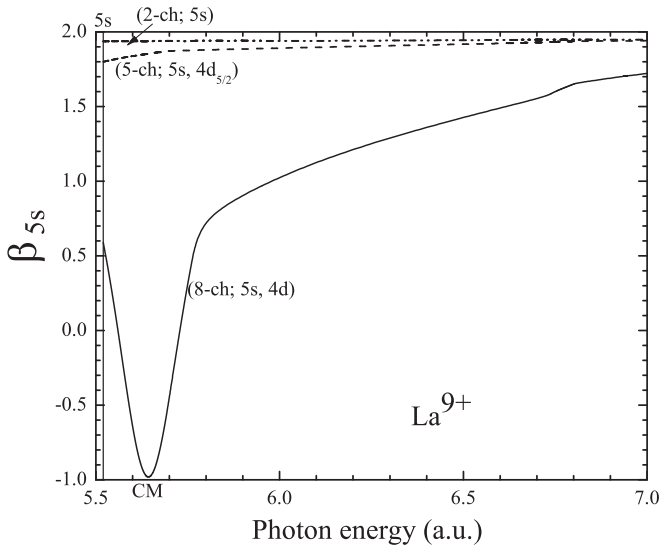


FIG. 4. Same as Fig. 2 but for  $\text{La}^{9+}$  in the 5.5 to 7.0 a.u. energy range.

coupling between the  $4d$  channels with each other and with those from  $5s$  subshell induces a second above-threshold Cooper minimum. It is quite evident that, in this case too, interchannel coupling is crucial for a correct determination of the location of the Cooper minimum and, thereby, the photoionization cross section.

Earlier photoionization studies reported that, along an isonuclear sequence, inner-shell cross sections remain unchanged, except for a shift in the ionization thresholds [15–17] as long as only electrons with higher principal quantum numbers were removed. In going from  $\text{La}^{3+}$  to  $\text{La}^{9+}$  the  $5p$  electrons are removed and, since  $5s$  photoionization is being studied, electrons of the same principal quantum number are being removed. Thus, we have extended the studies on  $5s$  photoionization from  $\text{La}^{3+}$  (13 channels) and  $\text{La}^{9+}$  (8 channels) up to 10 a.u., shown in Figs. 5 and 6, for the cross section and angular distribution asymmetry parameter, respectively. Note that, in these figures, the data for  $\text{La}^{3+}$  between 3 and 5.2 a.u. represent an approximate background cross section in a region that is dominated by resonances, as mentioned earlier. As seen from Fig. 5, the  $\text{La}^{3+}$  cross-section curve does not coincide with that for the  $\text{La}^{9+}$  cross section at or above the threshold of the latter, as expected. The removal of the  $5p$  electrons from  $\text{La}^{3+}$  has a significant effect on the  $5s$  photoionization cross section, because the orbital size of the two subshells is roughly the same (determined primarily by principal quantum number) so that the screening of the  $5s$  changes considerably in going from  $\text{La}^{3+}$  to  $\text{La}^{9+}$ . The positions of the Cooper minima in the  $5s$  cross sections above the  $4d$  thresholds in  $\text{La}^{3+}$  and  $\text{La}^{9+}$  occur at different energies, resulting in the two significant differences in the cross sections. On the other hand, although the angular distribution asymmetry parameter,  $\beta$ , for these two cases exhibits similar features, they are, however, rather different in detail, as shown by Fig. 6. The primary cause of the large difference in the  $\beta$ 's for the two cases is the energy dependence of the position of the Cooper minima.

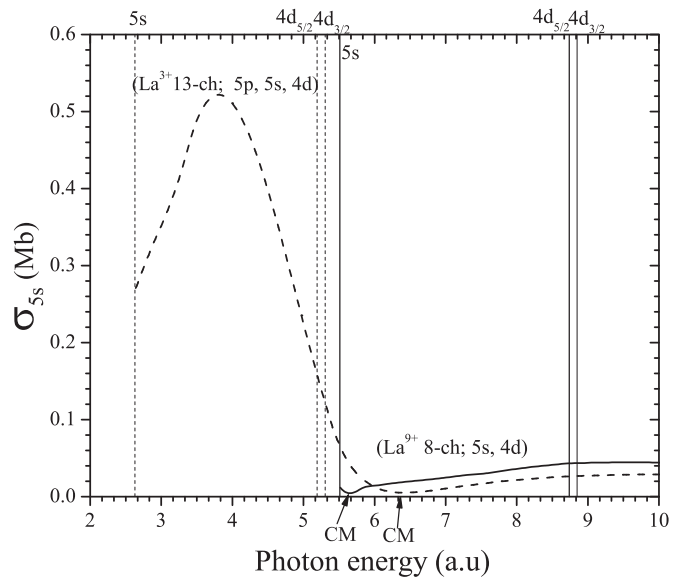


FIG. 5. Same as Fig. 1 but for  $\text{La}^{3+}$  and  $\text{La}^{9+}$ . The lower thresholds are for  $\text{La}^{3+}$  and the higher for  $\text{La}^{9+}$ .

Photoionization calculations have also been performed for the  $4d$  subshells of  $\text{La}^{3+}$ ,  $\text{La}^{9+}$  and  $\text{La}^{11+}$ , and the results for the  $4d$  photoionization cross sections (the sum of  $4d_{5/2}$  and  $4d_{3/2}$ ) for each of the ions are shown in Fig. 7. The outstanding feature of this comparison is that the  $4d$  cross sections for  $\text{La}^{3+}$ ,  $\text{La}^{9+}$ , and  $\text{La}^{11+}$  are almost exactly the same, except for an increase in the ionization thresholds. Removal of electrons from the  $5p$  subshell leading to the formation of  $\text{La}^{9+}$ , and from the  $5p$  and  $5s$  subshells to form  $\text{La}^{11+}$  does not make any significant difference in the  $4d$  cross sections, as functions of photon energy, except for a shift of the respective thresholds to higher energies. This is because the charge density of the  $n = 5$  electrons that were removed approximate a spherical shell of negative charge, well outside the spatial extent of the

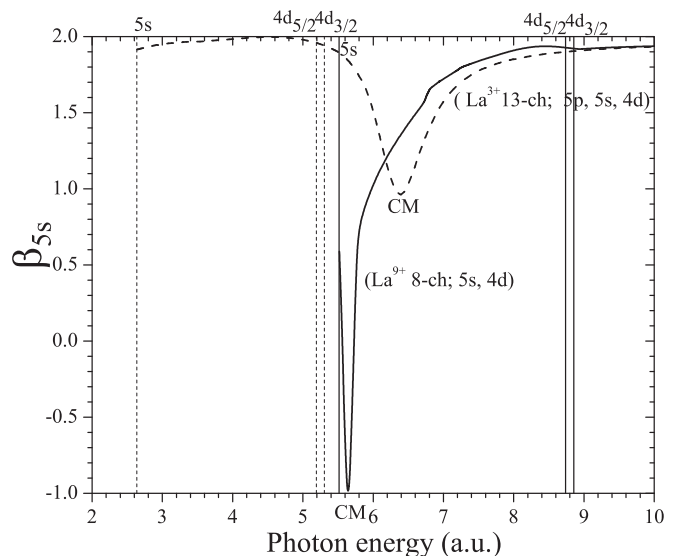


FIG. 6. Same as Fig. 2 but for  $\text{La}^{3+}$  and  $\text{La}^{9+}$ . The lower thresholds are for  $\text{La}^{3+}$  and the higher for  $\text{La}^{9+}$ .

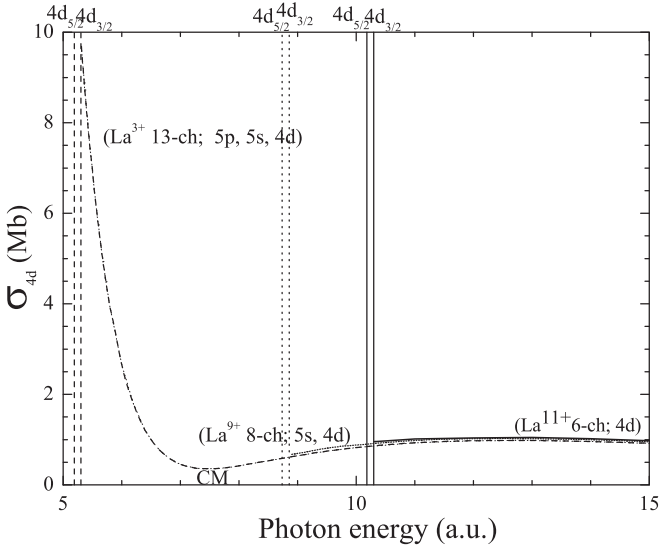


FIG. 7. Same as Fig. 1 but for the total  $4d$  cross sections ( $4d_{5/2} + 4d_{3/2}$ ) of  $\text{La}^{3+}$ ,  $\text{La}^{9+}$ , and  $\text{La}^{11+}$ , with the  $4d$  thresholds of each of the respective ion stages given.

$4d$  orbitals, and a spherical shell of negative charge exerts no force on charges in its interior; its only effect is to increase the potential inside by a constant amount which accounts for the shift in thresholds with increasing stage of ionization [15–17]. In addition, it is of note that the individual  $4d_{5/2}$  and  $4d_{3/2}$  cross sections each lie along the same curve (not shown), as a function of photon energy, not just the total  $4d$  cross section.

The  $4d$  cross sections for  $\text{La}^{9+}$  and  $\text{La}^{11+}$  are seen to increase slightly from their respective  $4d$  thresholds. However, this increase in the cross section is not due to the centrifugal barrier, as one might suspect. There is no delayed maximum (shape resonance) in the continuum for the  $\text{La}^{3+}$   $4d$  cross section caused by the centrifugal potential barrier, similar to the absence of the same for  $\text{Ba}^{2+}$  [24,35]; the attractive Coulomb potential here is strong enough to pull the shape resonance into the discrete region of the  $4d$  spectrum. The  $\text{La}^{3+}$  cross section goes through a Cooper minimum at  $\sim 7.5$  a.u. and then merges with the profiles for  $\text{La}^{9+}$  and  $\text{La}^{11+}$  cross sections, as seen in Fig. 7. The slight increase of the  $4d$  cross sections above the thresholds in  $\text{La}^{9+}$  and  $\text{La}^{11+}$  can therefore be attributed to the “recovery” from their respective Cooper minima in the discrete region.

In earlier work on  $\text{La}^{3+}$  by Cheng and Johnson [24], where only the six dipole channels from  $4d_{5/2}$  and  $4d_{3/2}$  were coupled, the Cooper minimum in the  $4d$  cross section was reported at  $\sim 6.98$  a.u. Our 6-channel result (not shown) and 13-channel results show this Cooper minimum at a slightly higher energy ( $\sim 7.5$  a.u.); the slight difference is probably numerical, since we have used essentially the same code [21], the difference being only due to the somewhat finer energy grid size used in the present work.

The dipole angular distribution asymmetry parameter for the  $4d$  subshell for the La isonuclear sequence, averaged over spin-orbit split states, is given by [32,33]

$$\beta_{4d} = \frac{\sigma_{4d5/2}\beta_{4d5/2} + \sigma_{4d3/2}\beta_{4d3/2}}{\sigma_{4d5/2} + \sigma_{4d3/2}}. \quad (3)$$

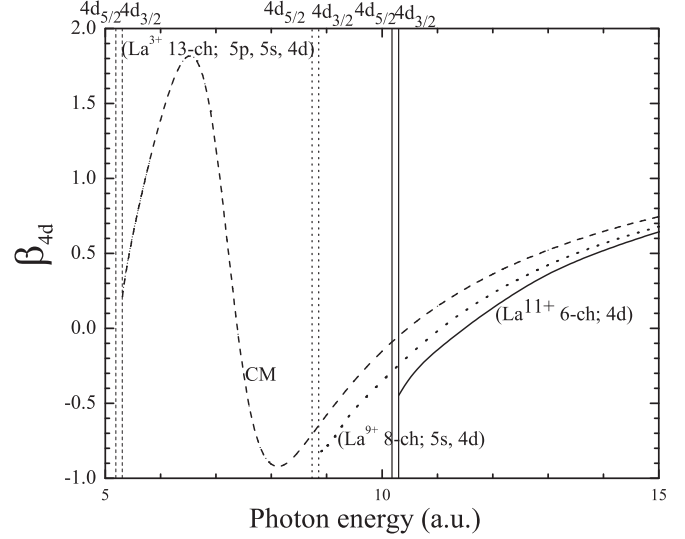


FIG. 8. Same as Fig. 2 but for the effective  $4d$   $\beta$ 's of  $\text{La}^{3+}$ ,  $\text{La}^{9+}$ , and  $\text{La}^{11+}$  (as defined in text), with the  $4d$  thresholds of each of the respective ion stages given.

The calculated  $\beta$ 's are shown in Fig. 8. For  $\text{La}^{3+}$ , the calculated value of  $\beta_{4d}$  at the Cooper minimum is  $-0.303$ , which is different from the result one would expect from the nonrelativistic value of 0.2 [36]. The behavior of  $\beta_{4d}$  for the three ions in the threshold region is slightly different, but with increasing photon energy, these differences become smaller and will disappear at high enough energies. This is because the Coulomb phase shifts in the angular distribution asymmetry parameter depend on the photoelectron kinetic energy, not photon energy, and the asymptotic charge of the residual ion [36,19]. At high enough energies, however, the Coulomb phase shifts become quite small and their effect on the  $\beta$  parameter is then negligible; i.e., the differences get smaller with increasing electron kinetic energy.

The branching ratios  $4d_{5/2}:4d_{3/2}$  for  $\text{La}^{3+}$ ,  $\text{La}^{9+}$ , and  $\text{La}^{11+}$  are shown in Fig. 9 and, since they are ratios of cross sections that are the same for each ion, as a function of photon energy, it is evident that the branching ratios must also lie along the same curve as seen. For  $\text{La}^{3+}$ , below the  $4d$  ionization thresholds of  $\text{La}^{9+}$  and  $\text{La}^{11+}$ , the branching ratio is smaller than the statistical value of 1.5, and it decreases to 1.12 at  $\sim 6.7$  a.u., below the  $4d_{5/2}$  Cooper minimum. The branching ratio then increases sharply to about 1.62, at a photon energy of  $\sim 8.8$  a.u., after which it starts to decrease again towards the statistical value of 1.5. The sharp increase near the Cooper minimum occurs because the  $4d_{5/2}$  cross section reaches its minimum value at a lower photon energy than the  $4d_{3/2}$  cross section, which is a consequence of the Cooper minimum in the  $4d_{5/2}$  channel lying at a lower photon energy than for the  $4d_{3/2}$ . This is the manifestation of a general rule that, for Cooper minima arising from spin-orbit split states, the minimum for the higher  $j$  state always occurs at lower photon energies [37]. In any case, since the  $4d$  thresholds of  $\text{La}^{9+}$  and  $\text{La}^{11+}$  are well above the Cooper minima, the branching ratios show only a minor departure from the statistical value for these ions.

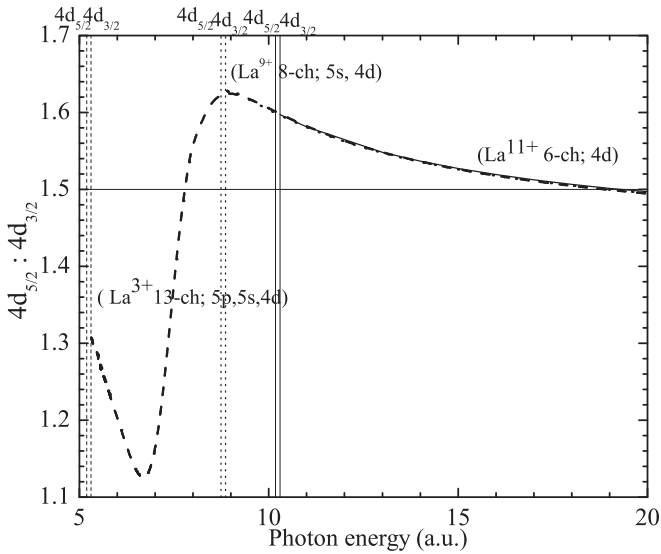


FIG. 9.  $4d_{5/2} : 4d_{3/2}$  branching ratios for  $\text{La}^{3+}$ ,  $\text{La}^{9+}$ , and  $\text{La}^{11+}$  as functions of photon energy with the  $4d$  thresholds of each of the respective ion stage given.

#### IV. CONCLUSIONS

Theoretical studies of the photoionization of near-outer subshells of three ions of the La isonuclear sequence have demonstrated that correlation in the form of interchannel coupling is of great importance, even for rather highly charged ions. This was found to be particularly true in the vicinity

of Cooper minima in the dipole matrix elements where the inclusion of interchannel coupling is critical; in fact it was seen that interchannel coupling induced Cooper minima where none appear without the coupling.

It was also confirmed that the photoionization cross section of a given subshell was affected significantly by removal of outer-shell electrons with the same principal quantum number, but essentially unaffected by the removal of electrons with higher  $n$  as was found in the past in other cases [15–17]. However, an extension to that phenomenology was found; with the introduction of relativistic interactions, it applies individually to each  $j$  state of a spin-orbit split subshell, specifically  $4d_{5/2}$  and  $4d_{3/2}$  in the present work.

Finally, it was demonstrated that there were various near-threshold effects owing to the relativistic splitting of the thresholds in the  $4d$  case. Furthermore, dramatic deviations of the  $\beta$  parameter from the nonrelativistic value of 2 were found in broad energy regions around the Cooper minima. Thus it is evident that, for accuracy in the calculation of photoionization parameters in this region of the Periodic Table, relativistic calculations must be employed.

#### ACKNOWLEDGMENTS

This work was partially supported by the Department of Science and Technology, Ministry of Science and Technology, Government of India. We also acknowledge support under the FP7-PEOPLE-2012-IRSES scheme for facilitating exchange between DCU and IITM researchers. S.T.M. was supported by the U.S. DOE, Office of Chemical Sciences.

- 
- [1] V. N. Polkovnikov, N. N. Salashchenko, S. D. Starikov, and N. I. Chkhalo, *Bull. Russ. Acad. Sci.: Phys.* **78**, 61 (2014).
- [2] B. Li, P. Dunne, T. Higashiguchi, T. Otsuka, N. Yugami, W. Jiang, A. Endo, and G. O'Sullivan, *Appl. Phys. Lett.* **99**, 231502 (2011).
- [3] N. Tatsumura, S. Yamamura, T. Ozawa, K. Horioka, and T. Kawamura, *Phys. Plasmas* **20**, 083304 (2013).
- [4] J.-M. Bizau, J.-M. Esteva, D. Cubaynes, F. J. Wuilleumier, C. Blancard, A. C. La Fontaine, C. Couillaud, J. Lachkar, R. Marmoret, C. Rémond, J. Bruneau, D. Hitz, P. Ludwig, and M. Delaunay, *Phys. Rev. Lett.* **84**, 435 (2000).
- [5] Y. Y. Qi, Y. Wu, and J. G. Wang, *Phys. Plasmas* **16**, 033507 (2009).
- [6] K. Davidson, *Astrophys. J.* **171**, 213 (1972).
- [7] J. Colgan, H. L. Zhang, and C. J. Fontes, *Phys. Rev. A* **77**, 062704 (2008).
- [8] C. E. Theodosiou, S. T. Manson, and M. Inokuti, *Phys. Rev. A* **34**, 943 (1986).
- [9] J. A. Shaw, M. S. Pindzola, M. Steidl, K. Aichele, U. Hartenfeller, D. Hathiramani, F. Scheuermann, M. Westermann, and E. Salzborn, *Phys. Rev. A* **63**, 032709 (2001).
- [10] J. M. Bizau, C. Blancard, D. Cubaynes, F. Folkmann, J. P. Champeaux, J. L. Lemaire, and F. J. Wuilleumier, *Phys. Rev. A* **73**, 022718 (2006).
- [11] A. Cummings, C. McGuinness, G. O'Sullivan, J. T. Costello, J. P. Mosnier, and E. T. Kennedy, *Phys. Rev. A* **63**, 022702 (2001).
- [12] J.-M. Bizau, D. Cubaynes, J.-M. Esteva, F. J. Wuilleumier, C. Blancard, J. Bruneau, J. P. Champeaux, A. C. La Fontaine, C. Couillaud, R. Marmoret, C. Rémond, D. Hitz, M. Delaunay, N. Haque, P. C. Deshmukh, H.-L. Zhou, and S. T. Manson, *Phys. Rev. Lett.* **87**, 273002 (2001).
- [13] N. El Hassan, J. M. Bizau, C. Blancard, P. Cossé, D. Cubaynes, G. Faussurier, and F. Folkmann, *Phys. Rev. A* **79**, 033415 (2009).
- [14] M. Habibi, D. A. Esteves, R. A. Phaneuf, A. L. D. Kilcoyne, A. Aguilar, and C. Cisneros, *Phys. Rev. A* **80**, 033407 (2009).
- [15] D. W. Missavage, S. T. Manson, and G. R. Daum, *Phys. Rev. A* **15**, 1001 (1977).
- [16] R. F. Reilman and S. T. Manson, *Phys. Rev. A* **18**, 2124 (1978).
- [17] K. D. Chao and S. T. Manson, *Phys. Rev. A* **24**, 2481 (1981).
- [18] G. Nasreen, S. T. Manson, and P. C. Deshmukh, *Phys. Rev. A* **40**, 6091 (1989).
- [19] G. B. Pradhan, J. Jose, P. C. Deshmukh, V. Radojević, and S. T. Manson, *Phys. Rev. A* **81**, 063401 (2010).
- [20] G. B. Pradhan, J. Jose, P. C. Deshmukh, V. Radojević, and S. T. Manson, *Phys. Rev. A* **80**, 053416 (2009).

- [21] W. R. Johnson and C. D. Lin, *Phys. Rev. A* **20**, 964 (1979); W. R. Johnson, C. D. Lin, K. T. Cheng, and C. M. Lee, *Phys. Scr.* **21**, 409 (1980).
- [22] D. Kilbane and G. O'Sullivan, *Phys. Rev. A* **82**, 062504 (2010).
- [23] C. M. Lee and W. R. Johnson, *Phys. Rev. A* **22**, 979 (1980).
- [24] K. T. Cheng and W. R. Johnson, *Phys. Rev. A* **28**, 2820 (1983).
- [25] U. Köble, L. Kiernan, J. T. Costello, J.-P. Mosnier, E. T. Kennedy, V. K. Ivanov, V. A. Kupchenko, and M. S. Shendrik, *Phys. Rev. Lett.* **74**, 2188 (1995).
- [26] N. Murphy, A. Cummings, P. Dunne, and G. O'Sullivan, *Phys. Rev. A* **75**, 032509 (2007).
- [27] A. Derevianko, W. R. Johnson, and K. T. Cheng, *At. Data Nucl. Data Tables* **73**, 153 (1999).
- [28] S. S. Kumar, T. Banerjee, P. C. Deshmukh, and S. T. Manson, *Phys. Rev. A* **79**, 043401 (2009).
- [29] T. Banerjee, P. C. Deshmukh, and S. T. Manson, *Phys. Rev. A* **75**, 042701 (2007).
- [30] H. R. Varma and P. C. Deshmukh, Photoabsorption processes in some free and confined atomic systems: Effects of correlation, relativistic interactions and confinement, Ph.D. thesis, IIT-Madras (Lambert Academic Publishing, Saarbrücken, Germany, 2011).
- [31] J. Jose, G. B. Pradhan, V. Radojević, S. T. Manson, and P. C. Deshmukh, *J. Phys. B* **44**, 195008 (2011).
- [32] T. E. H. Walker and J. T. Waber, *Phys. Rev. Lett.* **30**, 307 (1973).
- [33] S. T. Manson and A. F. Starace, *Rev. Mod. Phys.* **54**, 389 (1982).
- [34] V. Radojević, M. Kutzner, and H. P. Kelly, *Phys. Rev. A* **40**, 727 (1989).
- [35] T. B. Lucatorto, T. J. McIlrath, J. Sugar, and S. M. Younger, *Phys. Rev. Lett.* **47**, 1124 (1981).
- [36] S. T. Manson, *J. Electron. Spectrosc. Relat. Phenom.* **37**, 37 (1985).
- [37] Y. S. Kim, A. Ron, R. H. Pratt, B. R. Tambe, and S. T. Manson, *Phys. Rev. Lett.* **46**, 1326 (1981).